The effect of the microstructure on the static fatigue behaviour of Si_3N_4

WANG HONGJIE, WANG YONGLAN, JIN ZHIHAO, ZHOU HUIJIU
School of Material Science & Engineering, Xi'an Jiaotong University, Xi'an, 710049, People's Republic of China

The effect of the microstructure on the static fatigue behaviour of two Si_3N_4 samples containing different sintering aids has been studied. The results show that the static fatigue behaviours of the two samples are consistent with each other in various media, i.e. the rate of crack growth of both materials is greatest in water, followed by air, and then kerosene. A distinctive microstructure endows one of the samples with a higher fracture toughness. In turn this results in a higher crack propagation resistance and a longer service life at the same stress level.

1. Introduction

Silicon Nitride (Si_3N_4) possess a high heat-stability, hardness and wear resistance, oxidation resistance and corrosion resistance. When it is used as a structural component, it is important to have a method to appraising its service reliability and predict its service life. In addition, Si_3N_4 is a polycrystalline brittle material, whose microstructure i.e., grain size, crystal shape etc., can be adjusted to optimize its static fatigue behaviour. The effect of the microstructure on the static fatigue behaviour of two Si_3N_4 samples that contain different sintering aids is studied in this paper.

2. Experimental procedures

2.1. Theoretical background

The fatigue behaviour of a brittle material is characterized by subcritical crack growth. Generally under a static load, the dependence of the rate of crack growth on the stress intensity factor, K, is given by a simple power law [1];

$$V = A(K)^n \tag{1}$$

where A and n are constants, and n is the stress-corrosion exponent. For a type I crack on the surface of the material, the stress intensity factor K_I is given by:

$$K_I = Y\sigma_a a^{1/2} \tag{2}$$

where Y is a geometric factor, σ_a is the applied stress and a is the crack length. For a static loading test the lifetime t_r can be calculated by the integration of Equation 1 to yield:

$$t_f = B\sigma_a^{n-2}\sigma_a^{-n}[1-(\sigma_a/\sigma_c)^{n-2}] \tag{3}$$

where σ_c is the inherent strength, i.e., the strength in the absence of a subcritical crack extension, $B = 2/[AY^2(n-2)K_I\sigma^{n-2}]$ and is a constant which depends on the material and environment but, is independent of the applied load.

Since σ_a/σ_c is much smaller than 1, and the value of n for ceramic materials is generally higher, the value of $(\sigma_a/\sigma_c)^{n-2}$ is much smaller than 1. Thus Equation 3 can be simplified to:

$$t_r = B\sigma_a^{n-2}\sigma_a^{-n} \tag{4}$$

The log–log representation of Equation 4 is:

$$\log \sigma_a = (-1/n)\log t_f + (1/n)\log B + [(n-2)/n]\log \sigma_c \tag{5}$$

From Equation 5, it can be seen that the relationship between the applied load (σ_a) and the lifetime (t_f) can be fitted to a straight line on a log–log representation, whose slope is $(-1/n)$, and hence the stress-corrosion exponent n can be obtained.

2.2. Experimental details

Table I lists the sintering aids, sintering conditions and constituent phases in the two Si_3N_4 samples.

Specimens for the fatigue tests were prepared by grinding and polishing the sintered samples. Precracks were introduced at the centre of the test specimens before the fatigue tests were performed using a vickers indentor operated at a load of 196N in order to reduce the scatter of the experimental data. Experiments were performed with three-point bending in an in-house designed testing system. All the experiments were carried out at room temperature in three different media, namely H_2O, air and kerosene. Eight specimens of each material were tested at each static load and in each environment.

3. Results

3.1. Microstructure and toughness

Fig. 1(a and b) shows scanning electron micrographs of the two samples. From these micrographs, it can be seen that the main phase in both materials is columnar

0022–2461

β-Si_3N_4, but that the grain size in sample N2 is smaller than that of sample N1. In addition the ZrO_2 in sample N2 (the bright species in the micrographs) distributes on the grain boundaries in the form of small particles. Table II lists the fracture toughness, grain size, aspect ratio and the morphology of the samples used in this study. Due to the well-distributed microstructure and the dispersion of the ZrO_2 grains, sample N2 has the higher fracture toughness value.

TABLE I Preparation of the experimental samples

Material	Additives	Processing method	Main phase
N1	$Y_2O_3 + Al_2O_3$	Pressureless sintering	β
N2	$Y_2O_3 + Al_2O_3 + ZrO_2$	Pressureless sintering	$\beta + ZrO_2$

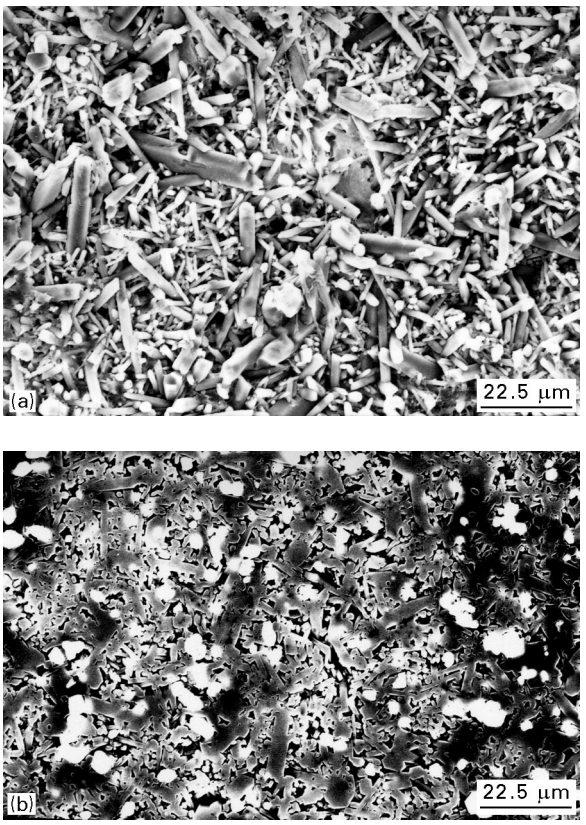

Figure 1 SEM micrographs of samples (a) N1 and (b) N2.

3.2. Static fatigue behaviour

Fig. 2(a–f) shows the static fatigue plots obtained in various environments for the two materials. The data were plotted in accordance with Equation 5 and the fatigue parameter n was estimated from the gradient of the line.

Table III lists the static fatigue parameters of the two materials, in the three media.

From Fig. 2(a–f) and Table III, we can see that the static fatigue parameters, n, of the two materials in the various media are much higher than those reported for oxide ceramics and glass-ceramics under the same conditions [5, 6], which indicates that the static fatigue behaviour of Si_3N_4 is far superior to that of oxide- and glass-ceramics. Thus the oxide- and glass-ceramics are more susceptible to slow crack growth than Si_3N_4 in the investigated media at room temperature thus limiting its service life. However, from Table III, we can see that the static fatigue parameters of the two materials in air, water and kerosene are different from one another, so we applied a relationship between log V and log K derived from Equation 1, and for the sake of convenience substituted the parameters n, Ln B and Ln A obtained from the experiment (Fig. 3).

From Fig. 3(a and b) we can conclude that the variations in the crack growth rate of the two materials follow the same pattern in all the various environments, i.e., the rate of crack growth at the same stress intensity factor for the material is greatest in water, followed by air and then kerosene. This shows that the tested materials all appear to be sensitive to the environment. Water is known to chemisorb onto strained bonds in SiO_2 and Al_2O_3, and this is the mechanism responsible for the occurrence of static fatigue in these materials [7–9]. However, the viscosity of kerosene inhibits this chemisorption reaction, and thus decreases the crack growth rate. At the same time, from

TABLE II Mechanical and microstructural properties of the materials

Material	σ_b^a(MPa)	K_{IC}^b(MPa m$^{1/2}$)^b	Aspect ratio	Morphology
N1	700	6.25	7	Columnar
N2	579	7.94	5	Columnar and equaxial grain

[a] Determined by three-point bending method
[b] Determined by indentation method (196N)

TABLE III The static fatigue parameters for samples N1 and N2 obtained in the three investigated media

	n		Ln B		Ln A	
	N1	N2	N1	N2	N1	N2
Air	647.8	1196.46	− 416.78	− 1718.19	− 223.62	− 843.46
Water	425.33	596.88	− 324.51	− 285.9	− 457.78	− 136.64
Kerosene	84.25	228.13	− 41.19	− 147.89	− 114.40	− 141.71

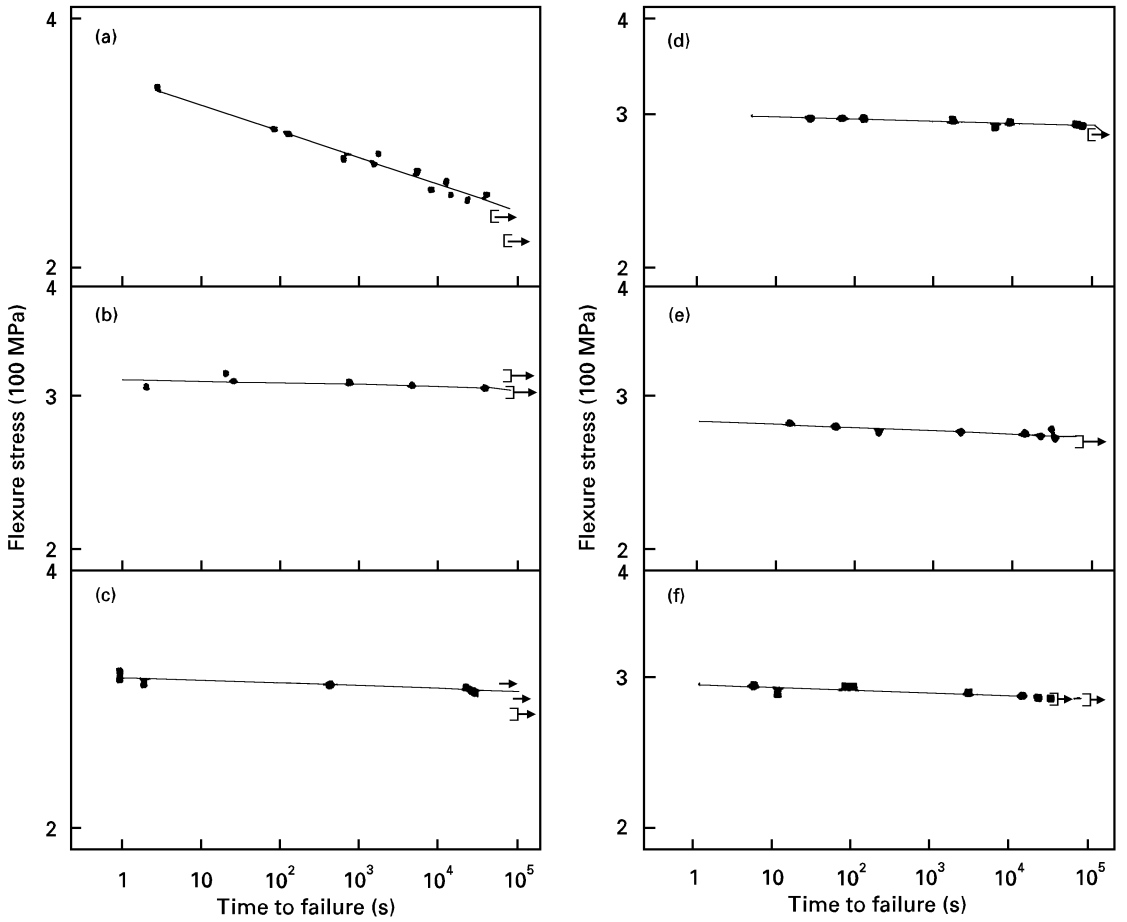

Figure 2 The static fatigue data for sample N1 (a) in kerosene, (b) in water and (c) in air and also sample N2 in (d) kerosene, (e) water and (f) air.

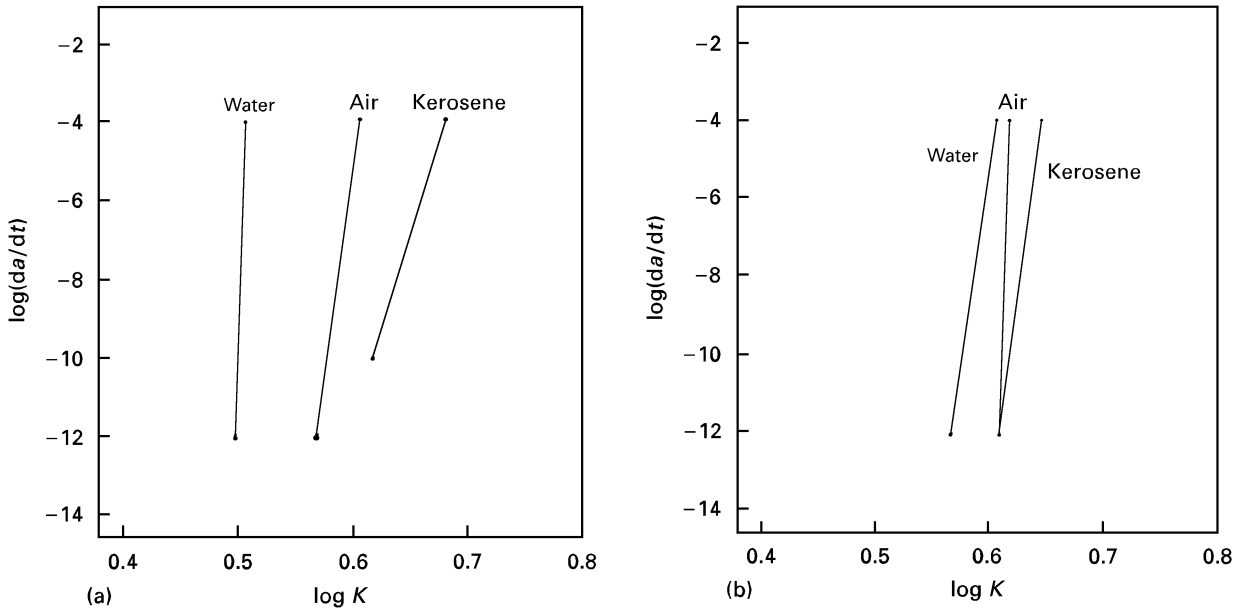

Figure 3 log V –log K curves obtained in the various media for (a) sample N1 and (b) sample N2.

Fig. 3(b), we can see that the log V –log K plots for the N2 sample contained in the three media are very close to one another, and each n value for the N2 sample in each medium is higher than that of the N1 sample in the same medium (see Table III). This indicates that the N2 sample has a higher crack propagation resistance and is more insensitive to the environmental medium.

4. Discussion

The static fatigue behaviour in air of the N1 and N2 samples were compared with respect to their log V–log K plots. Since the fracture toughness (K_{IC}) values of these materials are different, the K value normalization method was used, i.e., K/K_{IC} is substituted for K in the log V –log K curve (Fig. 4). From Fig. 4, we can see that the rate of crack growth of the

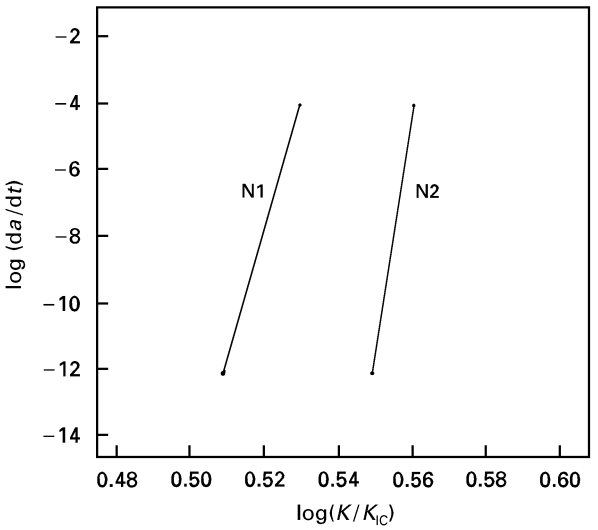

Figure 4 The static fatigue behaviour of the N1 and N2 samples in air.

N1 sample is higher than that of the N2 sample when the relative stress intensity factor K_I/K_{IC} is defined.

4.1. The effect of the microstructure on the static fatigue behaviour

It is known that the static fatigue process is in fact a stress corrosion process. Yamanchi [3] has investigated the fatigue behaviour of various ceramics and found that the static fatigue resistance in non-oxide ceramics decreased with an increase in the amount of an intergranular glassy phase. This result implies that the stress corrosion cracking is related not to the matrix itself, but to the interface between the matrix and the glassy phase at the grain boundary. In sample N2 the ZrO_2 exists as small particles that are well-distributed among the glassy phase, so when the stress corrosion crack caused by the medium meets these particles, the crack propagation is hindered. The crack is either stopped or its path is deflected, so the static fatigue crack propagation of the N2 sample is less sensitive to the environment than is the N1 sample.

4.2. The influence of the fracture toughness

From the results presented in this paper, we can see that the fracture toughness, and in particular the static fatigue stress corrosion exponent n are strongly influenced by the microstructure. This is consistant with reports in the literature on Al_2O_3 [10, 11] but is inconsistant with data reported for transformation toughened ZrO_2 [12]. This may be the result of a different toughening mechanisms. Gune *et al.* [4] have investigated the relationship between the fracture toughness and the n value of some ceramics and shown that:

$$n = cK_{IC} \tag{6}$$

where c is a constant. From this Equation 4 can be rewritten as:

$$t_f = B\sigma_a^{-cK_{IC}} \tag{7}$$

therefore, it is concluded that the higher the fracture toughness the higher the n value and the longer the lifetime at the same stress level. The n value of the N2 sample is higher and the crack propagation resistance is also higher because of its higher fracture toughness.

5. Conclusions

(1) The two samples were obtained by a pressureless sintering technique and contained a glassy phase at the grain boundary. Their static fatigue behaviours are consistent with each other in the various media used in this study i.e., the rate of crack growth of the materials is greatest in water, followed by air, and finally kerosene.

(2) The crack propagation resistance of the N2 sample is higher than that of the N1 sample because of its distinctive microstructure. It is also less sensitive to the environment than is the N1 sample.

(3) The crack propagation resistance can be related to the microstructure via the expression $n = cK_{IC}$, i.e., the higher the fracture toughness, the higher the n value and the longer the lifetime at the same stress level.

References

1. A. G. EVANS and S. M. WIEDERHORN, *J. Mater. Sci.* **9** (1974) 270.
2. A. M. TERRY and W. F. STEPHEN, *J. Amer. Ceram. Soc.* **66** (1984) 284.
3. Y. YAMANCHI, *J. Ceram. Soc. Jpn.* **96** (1988) 885.
4. C. GUEN and H. SUSUMU, *J. Mater. Sci.* **28** (1993) 5931.
5. QIAO GUANJUN, Ph.D. thesis Xi′an Jiaotong University, (1996).
6. WANG JIAN, Ph.D. thesis Xi′an Jiaotong University (1995).
7. S. M. WIEDERHORN, S. W. FREIMAN, E.R. FULLER, Jr. and C. J. SIMMONS, *J. Mater. Sci.* **17** (1982) 3460.
8. T. A. MICHALSKE and S. W. FREIMAN, *J. Amer. Ceram. Soc.* **66** (1983) 284.
9. T. A. MICHALSKE and B. C. BUNLER, *J. Appl. Phys.* **56** (1984) 2686.
10. M. V. SWAIN, *Mater. Forum* **9** (1986) 34.
11. B. J. PLETTA and S. M. WIEDERHORN, *J. Mater. Sci.* **17** (1982) 1247.

Received 20 March
and accepted 19 December 1996